The Abdus Salam
International Centre for Theoretical Physics

United Nations
Educational, Scientific and
Cultural Organization

IAEA
International Atomic Energy Agency

2015-18

Joint ICTP/IAEA Workshop on Advanced Simulation and Modelling for Ion Beam Analysis

23 - 27 February 2009

Characterisation of Inhomogeneous Inclusions in Darwin Glass using IBA

C. Jeynes
University of Surrey Ion Beam Centre
U.K.

*Nucl.Instrum.*Methods, 2009 (*in press*)

Characterisation of Inhomogeneous Inclusions in Darwin Glass using IBA

M. J.Bailey[1], K. T. Howard[2], K. J. Kirkby[1] and C. Jeynes[1a]

[1]University of Surrey Ion Beam Centre, Guildford, GU2 7XH, England

[2] Impacts and Astromaterials Research Centre (IARC), Mineralogy Department, The Natural History Museum, London, England

Abstract

Darwin glass is an impact glass resulting from the melting of local rocks during the meteorite impact that formed the 1.2 km diameter Darwin Crater in western Tasmania. These glass samples have small spheroidal inclusions, typically a few tens of microns in diameter, that are of great interest to the geologists. We have analysed one such inclusion in detail with proton microbeam ion beam analysis (IBA). A highly heterogeneous composition is observed, both laterally and in depth, by using self-consistent fitting of photon emission and particle backscattering spectra. With various proton energies near 2 MeV we excite the $^{12}C(p,p)^{12}C$ resonance at 1734 keV at various depths, and thus we can probe both the C concentration, and also the energy straggling of the proton beam as a function of depth which gives information on the sample structure. This inclusion had an *average* composition of (C, O, Si) = (28, 56, 16) mol% with S, K, Ca, Ti and Fe as minor elements and Cr, Mn, Ni, Cu, Zn and Br as trace elements. This composition included, at specific points, an elemental depth profile and a density variation with depth consistent with discrete quartz.crystals a few microns in size.

Keywords: PIXE, RBS, EBS, impact glass, Simulated Annealing, 3D analysis, silica

PACS:

82.80.Yc	Rutherford backscattering (RBS), and other methods of chemical analysis
82.80.Ej	X-ray, Mössbauer, and other γ-ray spectroscopic analysis methods
96.30.Za	Meteors, meteorites and tektites
91.67.Gy	Chemical composition (geology)
81.05.Kf	Glasses
89.60.Gg	Impact of natural and man-made disasters
61.05.Np	Atom, molecule, and ion scattering (for structure determination only)
68.35.Ct	Interface structure and roughness

---

[a] Corresponding author: email c.jeynes@surrey.ac.uk, tel +44 1483 689829, http://www.surreyibc.ac.uk

Introduction

Impact glasses are formed by the shock melting of target rocks at pressures > 45 GPa during the initial stages of meteorite crater formation. The molten rock is blasted out of the expanding crater cavity and solidifies in flight before raining down across the landscape. Impact glasses inherit the composition of the target rocks from which they form. Darwin glass is a siliceous impact glass formed from impact melting of quartzite and shale [1]. The glass is found across a 400 km^2-strewn field in western Tasmania, Australia [1,2]. Argon isotope dating of the glass indicates that it was formed around 800 thousand years ago [3]. The 1.2 km diameter Darwin Crater, a buried structure located in a narrow rain forested valley, is the source of the glass [1,2]. Relative to the size of the source crater, this is the most abundant and widely dispersed impact glass on Earth [4].

Recently, spheroidal inclusions were discovered within the glass. The study of these inclusions will allow a better understanding of its formation and the nature of impact events. Ion beam analysis methods such as Particle Induced X-ray Emission (PIXE) and Elastic Backscattering Spectrometry (EBS), have the required spatial resolution, and are also non-destructive. EBS includes the special case of Rutherford backscattering (RBS) for which the scattering cross-sections are given by the Coulomb potential.

The present work demonstrates a quantitative three-dimensional (3D) analysis of these highly non-uniform samples, with depth resolution also available for the minor and trace elements. The self-consistent PIXE/RBS/EBS analysis essential for this analysis is very new [5, 6, 7]. Probing the density variation of inhomogeneous samples by RBS using the consequent energy straggling to determine the size of the inhomogeneities has been done recently by Stoquert & Szörenyi using an analytical code [8], and Tosaki has used a Monte Carlo code to calculate the effect on C resonance signals in EBS spectra of the same excess energy straggling from density variations in graphite samples [9]. Barradas has used Stoquert & Szörenyi's algorithm to characterise nanoparticles by RBS [10, 11], and also demonstrated that the excess energy straggling can be calculated correctly with an analytical code in the presence of sharp EBS resonances [12]. We use the code of Barradas here, where the energy straggling of homogeneous samples is calculated from Bohr's (1915) formula with Chu's correction [13] and Tschalär's convolution with depth [14]. It was not necessary for these spectra to use Szilágyi's [15] accurate calculation of straggle as a function of depth.

In particular, we use Tosaki's method of probing the sample structure using the energy straggling as revealed here by the $^{12}C(p,p)^{12}C$ EBS resonance at 1734keV, which has a peak elastic scattering cross-section of 45 times Rutherford with our geometry. It is because the EBS resonance cross-section is so large at its peak that the measured spectrum reveals the actual energy distribution (and hence the energy straggling) of the beam at the resonance depth.

Materials and Methods

An inclusion of ~100 μm in diameter was picked from a sample of Darwin glass and embedded in a resin block which was then polished flat. It was studied by PIXE and RBS/EBS using a proton beam focussed to 4 x 4 μm^2 on the Surrey 2MV Tandetron [16]. The X-ray detector was a Si(Li) from e2v with 130 μm Be filter to exclude backscattered particles, at an angle to the beam of 45°, and with a solid angle of 30 msr. The particle detector was an old Si diode, with very poor resolution (50 keV) at a scattering angle of 25° and a solid angle of 50 msr.

Maps of the inclusion were produced using incident beam energies of 1.76, 1.91, 2.07 and 2.40 MeV to make use of the $^{12}C(p,p)^{12}C$ [17, 18] resonance at 1734 keV in this very C-rich sample; and at increasing exit angles to the PIXE detector of 45° (normal beam incidence), 63° and 77.7°. The PIXE maps were collected over times of up to fourteen hours using the list-mode feature of the OMDAQ software [19, 20] where the energy and beam position is recorded for each detected particle or photon. We have verified that these long irradiations did not cause significant changes to the sample by checking the change in the backscattering spectra from the resin between the first 10% and last 10% of a 14 hour run. We were looking particularly for changes between the surface and bulk of the sample, but found only very small changes in relative yield, at the 1% level.

An absolute energy calibration was used for the particle detector where the dead layer and non-ionising energy loss are taken into account and all the spectra have the same energy scale (in keV/channel). This can be done extremely precisely: Gurbich and Jeynes report an uncertainty in gain <0.1% [21]. In the present work the uncertainty is about 0.5%.

The depth profiles of the inclusions were determined by self-consistently fitting the PIXE and RBS/EBS spectra using the newly implemented PIXE module [22] of the DataFurnace code [23] (the latter is validated by an IAEA-sponsored intercomparison [24]). DataFurnace ("NDF") allows quantitative elemental concentration depth profiles to be extracted from the

backscattered particle energy spectrum, thus correctly determining the X-ray absorption. PIXE is implemented in DataFurnace using the algorithm of Reis [25]: note that other codes (such as GUPIX [26] which is implemented by OMDAQ) do not allow multiple layers containing the same element.

The fit of the backscattering and photon emission data uses the calculation engine NDFv9.2d [27]) of DataFurnace, with SRIM2003 stopping powers [28, 29, 30] and evaluated EBS cross-sections from SigmaCalc [31, 32] for O(p,p)O [33] and Si(p,p)Si [34], as well as C(p,p)C [17, 18]. DataFurnace has the best available convolutions in depth [35, 12] to reproduce the spectrum accurately in the vicinity of the resonances, although these have only a small effect for these spectra and were neglected (being computationally expensive). DataFurnace also implements the algorithm of Stoquert & Szörenyi [8] to calculate the effect on the energy straggling of density inhomogeneities. Chu straggling [13] with Tschalär scaling [14] was used, and it was necessary to assume heavy roughness [36, 37] to fit the EBS data. We have found that the present data could not be well fitted until we assumed that the silicon content is in the form of silica micro-inclusions of a certain size: this allows the energy straggle deep in the sample to also be fitted. Such inclusions are consistent with *in-situ* micro-XRD (X-ray diffraction: this will be reported separately) indicating the presence of crystalline SiO_2 (quartz micro-inclusions).

DataFurnace is a *fitting* code which can use the simulated annealing algorithm to effect global minimisation [23] (although these tools are not currently available for rough samples with inclusions). For these samples it is essential to restrict the parameter space searched by using "molecules" as *logical elements* (see discussion in [23]), where "molecule" refers to the calculational expedient of correlating elements in specific ratios, and does not refer to the chemistry of the sample: of course, IBA carries no chemical information.

DataFurnace also implements *sub*-"molecules" [27], which allow, for a single logical element, the independent simultaneous fitting of the major element stoichiometry (the C/O ratio) and the major:minor element ratio (C/Si) where the average minor and trace element stoichiometry is initially determined from the PIXE data. For the location of the quartz micro-inclusion, three logical elements were used apart from C & O: "molecules" representing the quartz, the resin, and the average minor and trace element content where the spectra are actually calculated with 9 or more real elements.

Results

One inclusion was selected for detailed study. Figure 1 shows the spatial distribution of some of the elements (Si, Fe and Cu) detected in this inclusion, which also contains Al, P, S, K, Ca, Ti, Cr, Mn, Br, Sr, Y, Zr, Bi, Cu, Zn, Ni (not shown here). These maps demonstrate the highly heterogeneous nature of the inclusion, with "hotspots" of different elements present. We will show both qualitatively and quantitatively that at least some of these "hotspots" are discrete micro-inclusions.

In Figure 2, PIXE maps for Ti taken at various beam incident angles are presented. As the sample is tilted, X-rays coming from features deep in the sample ("hotspot" marked with large circle) will move towards the right of the maps (so called stereo imaging), whereas X-rays coming from features at the surface (small circle) will stay static. This Ti "hotspot" is buried 25 μm deep. Similar effects were noted for Si and Fe micro-inclusions.

Since the presence of quartz was identified in the inclusion from XRD, the Si "hotspot" together with the adjacent Si-poor region shown in Figure 1 was selected for quantitative analysis. Figure 3 directly compares spectra from the resin with the Si-rich and Si-poor regions and shows the dramatic difference in the C signal at the resonance depth for the 1.91 MeV spectra (about 4 μm into this material). The $^{12}C(p,p)^{12}C$ resonance at 1734 keV probes the C content at this depth, and *also* probes the density variation in the shallower layers since the energy straggling is determined by these layers.

Spectra from the resin (Fig.4) are well fitted with a single "molecule":

(C 8261 O 1692 Cl 40) 99885 (Si 696 S 451) 116

(that is, assuming a uniform composition) where the C:O:Cl ratio is determined from the EBS spectra, the relative proportion of the elements in the minor sub-"molecule" is determined from the PIXE spectra (not shown), and the relative solid angles of the photon and particle detectors is detemined from the common Cl signal. It is interesting that these EBS spectra can be used to precisely determine the Cl content near the surface, which requires that the pulse pileup shown in Fig.4 must be accurately determined (DataFurnace uses the algorithm of Wielopolsky & Gardner [38]) and that the Cl scattering cross-section is well-known for these energies (demonstrated to be Rutherford by Bogdanović *et al* [39]). We can demonstrate that the near-surface region is characteristic of the bulk, and therefore that we can use the near-surface O and Cl signals, where there is no C background (or O

background for Cl), for the C/O and C/Cl ratios. The uncertainties of these ratios are both about 5% from counting statistics.

The average composition of the whole 100μm inclusion was fitted with the single "molecule":

$$(C28\ O27)553\ (Si1\ O2)433\ (S90\ K588\ Ca431\ Ti164\ Cr2\ Mn1\ Fe109\ Ni2\ Cu2\ Zn7\ Br10)14$$

The inclusion is extremely inhomogeneous, as seen in Figs.1 & 2, and this average composition is not characteristic of any part of it. However, the average silicon content of this whole inclusion is remarkably high, and its very high carbon content was unexpected.

Figure 5 shows one of the spectra, for 1.91 MeV, from the Si-poor region adjacent to the Si "hotspot", fitted two ways to give the extra straggling at the C resonance required to fit the data: using 6 μm spherical inclusions (Fig.5a) and just using roughness (Fig.5b). The roughness calculation depends on density variation at interfaces to generate excess straggling, but distributed inclusions do this all through the layers being traversed by the beam. Therefore it is reasonable that the spectral shape is different for the two models, and that the strong cross-section dip on the low energy side of the resonance is not fitted well in the second case. Note that the resonance lies at the depth of a large micro-inclusion (see Fig.5c).

Figure 6 shows a dramatically reduced C signal due to the presence of a large silica micro-inclusion (the same one as for Fig.5). In this case the concentration of silica is so high that modelling the straggle continuously through the layers with inclusions yields results no better than modelling the straggle with roughness.

Discussion

The inclusions are highly heterogeneous in composition and, unlike the bulk silicate glass they occur in, are composed predominantly of carbon. The analytical approach has allowed us to define not only the bulk composition of the inclusion but also to determine unambiguously the presence of buried elemental hot spots, effectively micro-inclusions within the carbonaceous inclusion. Obtaining both structural and 3D compositional information non-destructively makes ion beam analysis very attractive to the study of geological materials where inclusions are often of interest and may be hard to find and prepare: this sort of information is not otherwise available. XRF (or PIXE) tomography (with or without confocal techniques) can give 3D elemental distributions, but not the structural information..

Carbon and other elements common in the inclusions, such as K,Ca,Br,S, are considered volatile under impact conditions and are usually lost to a gas phase. Thus defining the origin of these inclusions will yield critical insights into the fate of volatiles during meteorite impacts. The presence of Br and S is interesting as these are common in reduced environments such as swamps. Elsewhere [40], the presence of abundant volatiles at the point of impact - in the form of a surface swamp - was used to explain the high abundance and wide distribution of Darwin glass. The Si hotspot is consistent with the stoichiometry of quartz (SiO_2), and the presence of quartz was also determined by micro-XRD. Work in progress is aimed at understanding the relationship between the quartz and the C rich host in which it is embedded. Co-genetic quartz formed during impact has not been described elsewhere.

Ion beam analysis techniques are interesting for these types of samples since elemental composition information is available both at high sensitivity and at high spatial resolution. PIXE has excellent elemental discrimination in most cases, and a sensitivity (at a few μg/g depending on the sample) orders of magnitude larger than that available for XRS (X-ray spectrometry) on the scanning electron microscope (SEM) since there is effectively no bremsstrahlung background. PIXE with a scanning ion microbeam also has a lateral resolution given by the spot size (not the particle energy, as in the SEM) which can be as small as 100nm.

On the other hand, although their mass resolution is quite poor the particle scattering techniques have an excellent depth resolution: 10 nm for a He beam and 100 nm for a proton beam being usually easily achievable. Moreover, the proton backscattering spectrum contains complete information about the sample: there is signal from all the sample atoms (except H) which means that the stoichiometry can be unambiguously determined as a function of depth. Particle scattering can be used for analyses whose traceable accuracy can be as good as 0.6% (1σ) [24], and the traceability in general is simple for particle scattering, with an accuracy of better than 5% usually available. For PIXE (as for SEM-EDS and for the same reasons) the traceable accuracy is not usually better than 10% (and sometimes much worse) although the precision can be excellent (<1%). For these highly inhomogeneous and irregular samples however, surface and interface topography and other effects degrade both traceability and accuracy for both PIXE and RBS/EBS.

The weakness of PIXE is that the depth resolution is normally very poor at a few microns; and the weakness of the particle scattering techniques is that the sensitivity is poor, being usually hard to get better than a few atomic %. But when, as here, we use the techniques

together, we obtain the sensitivity of PIXE together with the depth resolution and traceability of RBS/EBS. The photon emission and particle scattering techniques complement each other almost perfectly. We should point out, however, that the information depth of the particle scattering techniques is limited, in the present case to at most 20μm. This contrasts with the much larger information depths of the photon emission techniques (as in Fig.2).

In the present work this complementarity is very clear. The quartz micro-inclusion was located laterally by PIXE and in depth by RBS/EBS, with a volume of no more than 150μm^3 (400pg). We also show that 0.002 mol% on average of Cu is readily observed in the whole inclusion, and this level of sensitivity is also available with high lateral resolution.

We have been unable to get an excellent fit for the resonance buried about 4 μm deep in the Si-rich region (Fig.6) because we have no model capable of introducing sufficient energy straggling to wash out the very strong structure of the 1734 keV C resonance as the data require. But we are making use of the existing models for roughness [36, 37] and inclusions [8, 12] right up to (and beyond) their limits of validity. The general algorithm recently constructed by Molodtsov *et al* [41] can successfully model the severe roughness exhibited by samples such as these, including such roughness in the presence of EBS resonances (as in Beck *et al* [7]) showing directly that the energy straggling as a function of depth is indeed correctly calculated. If it can be applied to the "roughness" of internal interfaces, then the effects on IBA spectra of strong internal structures will be precisely calculable, and this resonance technique can be used accurately even for these remarkably complicated samples. However, the present analysis is unequivocal.

Conclusions

The analytical problem of locating these micro-inclusions is difficult since they do not have much direct contrast in backscattering. The PIXE analysis is very sensitive to minor and trace elements present, but these data cannot easily be used by themselves to characterise the micro-inclusions, and the stereo-pair location method is only qualitative and has poor depth resolution. We have shown that the data are consistent with silica micro-inclusions, located using the reduced yield from C at the $^{12}C(p,p)^{12}C$ 1734 keV resonance and sized using both the PIXE Si yield and the effect on the EBS straggling.

This type of microbeam data analysis is unprecedented: it cannot be completed without the correct, detailed and self-consistent handling of multiple particle backscattering spectra (including both Rutherford and non-Rutherford scattering) together with X-ray emission

spectra, which has only recently become available. Algorithms exist to extend the region of validity of the present treatment to be strictly correct even for these exceptionally complicated samples.

Microbeam IBA therefore has application to a wide class of samples that have been thought until now to be inaccessible to ion beam analysis. Integrated EBS/PIXE has been shown to have both high sensitivity and high spatial resolution in all three dimensions, and being non-destructive it is particularly valuable for rare samples such as these.

Acknowledgements

We thank EPSRC for support of this work under contract EP/D032210/1. We greatly appreciate the help of Dr.G.W.Grime in making facilities available in OMDAQ to manipulate the list mode files.

Figures

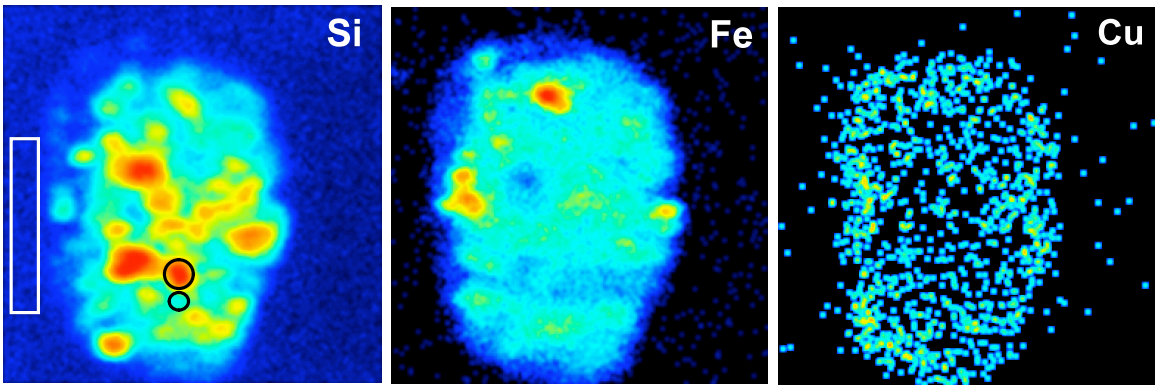

Figure 1. 2.4 MeV proton PIXE maps (150µm x 150µm) of the inclusion selected for detailed study showing the distribution of Si, Fe and Cu. Ti maps are shown in Figure 2. The three regions selected for quantitative analysis here are marked on the Si map: resin (oblong), Si-rich (large circle) and Si-poor (small circle). The Fe "hotspots" are also rich in Cr and Mn; Cu (correlated with Ni and Bi) is on the outside of the inclusion. Heterogeneous distributions are observed for Al, P, K, Ca, Zn, Br and Zr. Low levels of Ga, Ge, As, Rb and Sr are also observed.

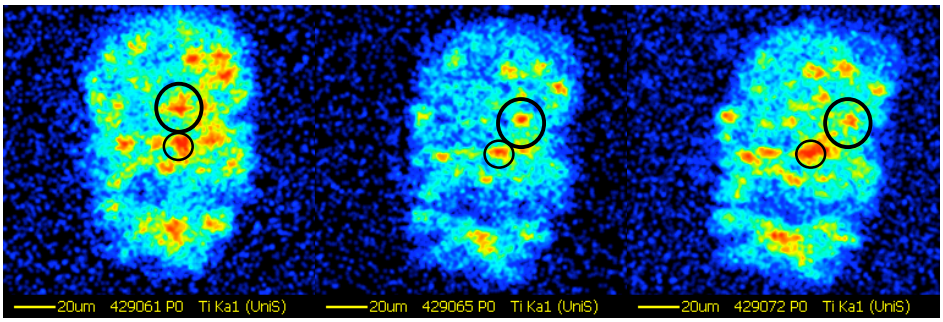

Figure 2. PIXE maps of the Ti for incident angles of 0°, -18.0° and -32.7°. "Hotspot" marked with large circle moves to the right and is buried 25 μm compared to a static feature (small circle).

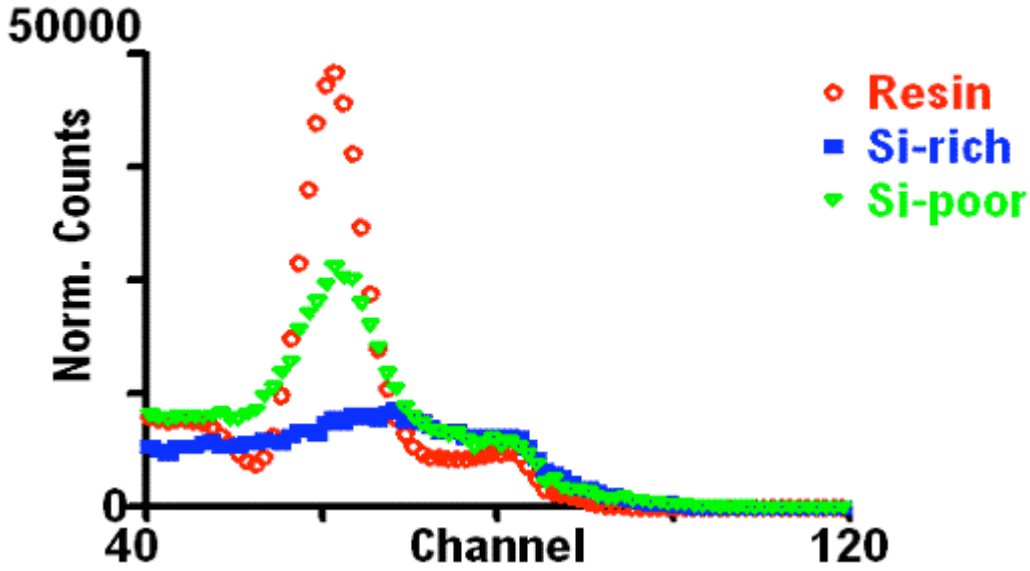

Fig.3: Comparison of 1.91 MeV spectra for the resin (circles), the Si-rich region (squares) and the Si-poor region (triangles). The spectrum for the resin, with no excess straggling due to roughness or density variation ("inclusions") reflects the shape of the $^{12}C(p,p)^{12}C$ resonance at a proton energy of 1734 keV. Notice the sharply reduced cross-section on the low energy side of the resonance. The lack of signal at the resonance peak is due to the lack of C in the sample; also excess straggling washes out the resonance strucure.

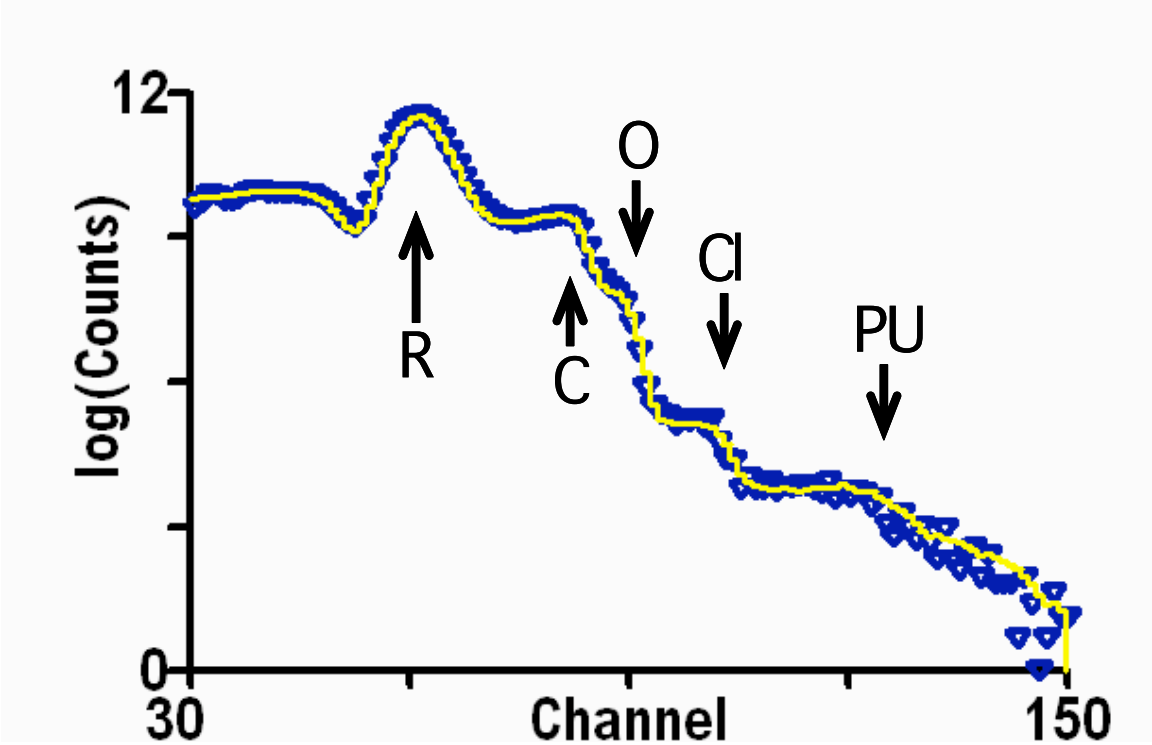

Figure 4: 1.91 MeV proton EBS spectrum and fit for resin (250nC collected charge). Ordinate scale is in natural logarithms. The C, O and Cl edges are marked, and the "edge" at channel 125 is pulse pileup from the C resonance ("PU"). The enhanced signal from the 1734 keV $^{12}C(p,p)^{12}C$ resonance peaks at channel 61 ("R").

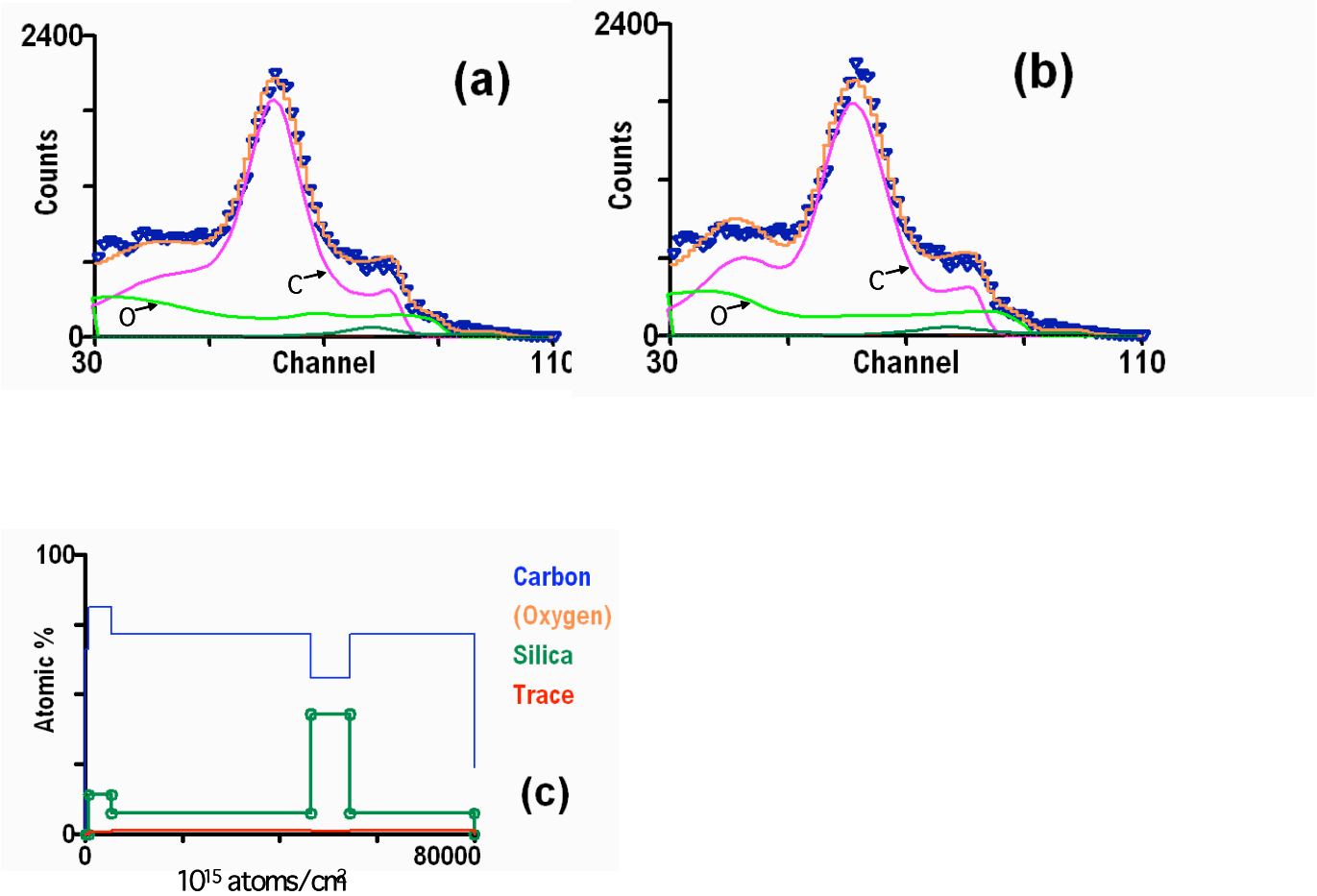

Figure 5: 1.91 MeV proton EBS spectra and fits for Si-poor region adjacent to Si-rich region (see Figure 6) . Partial spectra for C, O, Si (Si not marked) are shown, The $^{12}C(p,p)^{12}C$ resonance at 1734 keV is excited at a depth 4.10^{19} atoms/cm^2 (~4 µm) and peaks at channel 60 in the spectra.

a) excess straggling well calculated from spherical silica inclusions of diameter 6 µm,

b) excess straggling calculated from interface roughness does not wash out the structure of the C resonance at low energies,

c) Depth profile in absolute units equivalent to mass per unit area; the fits in a) & b) are calculated from this profile : profiles for carbon, a silica "molecule" (marked with circles) and a "molecule" containing the remaining trace elements are shown, oxygen is not shown for clarity.

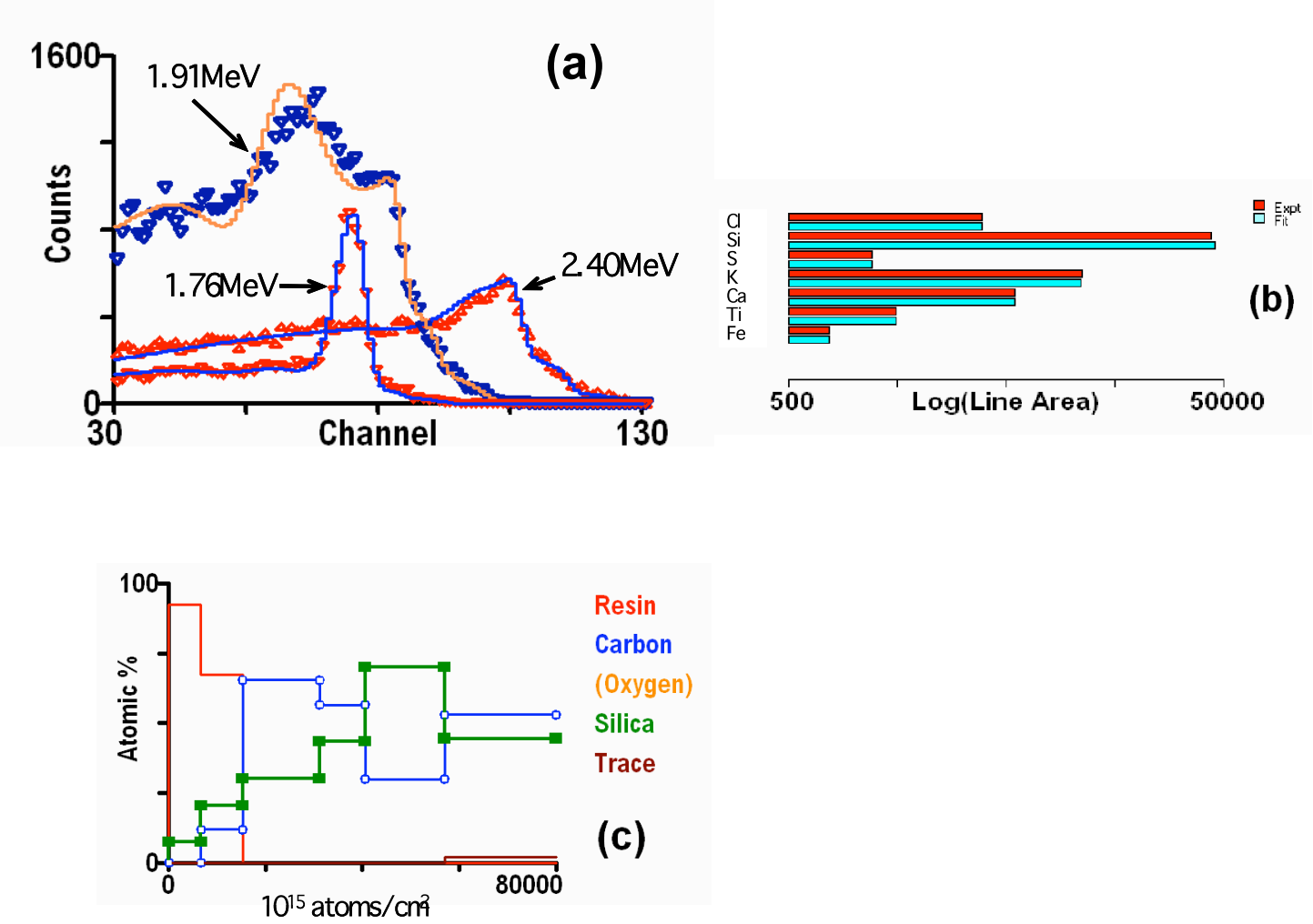

Figure 6: Depth profile for the Si-rich region extracted by self-consistent NDF fits for EBS and PIXE data. a) EBS spectra and fits for Si micro-inclusion for 1.76, 1.91, 2.4 MeV protons (collected charges respectively 2.65, 15.74, 6.41 nC): the $^{12}C(p,p)\,^{12}C$ resonance at 1734 keV is close to the surface for 1.76 MeV, buried at a depth of 4.10^{19} atoms/cm^2 (~4 µm) for 1.91 MeV and too deep to observe for 2.4 MeV; b) PIXE K-line areas extracted by GUPIX from spectra with NDF fit for 2.4 MeV protons; c) Fitted depth profile (carbon is marked with small open circles and the silica "molecule" is marked with large squares: no free O is needed for this fit). The high silica content in this profile is at a depth comparable to that in Figure 5. See text for discussion of the poorly fitting spectrum for 1.91 MeV.

References

1 K.T. Howard, P.W. Haines, The geology of Darwin Crater, western Tasmania, Australia, *Earth and Planetary Science Letters* **260** (2007) 328-339

2 K.T. Howard, Geochemistry of Darwin glass and target rocks from Darwin Crater, Tasmania, Australia, *Meteoritics and Planetary Science* **43** (2008), 473-496

3 C.H.Loh, K.T.Howard, S.L.Chung, S.Meffre, Laser-fusion $^{40}Ar/^{39}Ar$ Ages of Darwin Impact Glass, *Meteoritics and Planetary Science*, **37** (2002) 1555-1562

4 K.T. Howard, Distribution and Abundance of Darwin Impact Glass, *Proc. 3rd Int. Conf. on Large Meteorite Impacts, abstract.4057* (2003).

5 Carlos Pascual-Izarra, Nuno P. Barradas, Miguel A. Reis, Chris Jeynes, Michel Menu, Bertrand Lavedrine, Jean Jacques Ezrati, Stefan Röhrs, Towards truly simultaneous PIXE and RBS analysis of layered objects in cultural heritage. *Nucl. Instrum. Methods Phys. Res., Sect. B,* **261** (2007) 426-429

6 J.C.G. Jeynes, C. Jeynes, K.J. Kirkby, M. Rümmeli, S.R.P. Silva, RBS/EBS/PIXE measurement of single-walled carbon nanotube modification by nitric acid purification treatment, *Nucl. Instrum. Methods Phys. Res., Sect. B,* **266** (2008) 1569-1573

7 Beck L, Jeynes C, Barradas NP, Characterization of paint layers by simultaneous self-consistent fitting of RBS/PIXE spectra using simulated annealing, *Nucl. Instrum. Methods Phys. Res., Sect. B,* **266** (2008) 1871-1874

8 J.P. Stoquert, T. Szörenyi, Determination of the number and size of inhomogeneities in thin films by ion beam analysis, *Phys. Rev.B*, **66** (2002) 144108

9 M.Tosaki, Energy-loss straggling caused by the inhomogeneity of target material, *J.Appl.Phys.* **99(3)** (2006) 034905

10 N.P.Barradas, E.Alves, D.Babonneau, Characterisation of FePt nanoparticles in FePt/C multilayers, *Nucl. Instrum. Methods Phys. Res., Sect. B*, **219** (2004) 919-922

11 A.Fonseca, N.Franco, E.Alves, N.P.Barradas, J.P.Leitão, N.A.Sobolev, D.F.Banhart, H.Presting, V.V.Ulyanov, A.L.Nikiforov, High resolution backscattering studies of nanostructured magnetic and semiconducting materials, *Nucl. Instrum. Methods Phys. Res., Sect. B*, **241** (2005) 454-458

12 Barradas NP, Alves E, Jeynes C, Tosaki M, Accurate simulation of backscattering spectra in the presence of sharp resonances, *Nucl. Instrum. Methods Phys. Res., Sect. B,* **247** (2006) 381-389

13 Q. Yang, D.J. O'Connor, Zhonglie Wang, Empirical formulae for energy loss straggling of ions in matter, *Nucl. Instrum. Methods Phys. Res., Sect. B*, **61** (1991) 149-155

14 C. Tschalär, H.D. Maccabee, Energy-straggling measurements of heavy charged particles in thick absorbers, *Phys.Rev.*, **B1** (1970) 2863-2869

15 E. Szilágyi, F. Pászti, G. Amsel, Theoretical approximations for depth resolution calculations in IBA methods, *Nucl. Instrum. Methods Phys. Res., Sect. B,*,**100** (1995) 103-121

16 A. Simon, C. Jeynes, R. P. Webb, R. Finnis, Z. Tabatabaian, P. J. Sellin, M. B. H. Breese, D. F. Fellows, R. van den Broek, R. M. Gwilliam, The new Surrey ion beam analysis facility, *Nucl. Instrum. Methods Phys. Res., Sect. B,* **219-220** (2004) 405-409

17 A. F. Gurbich, Evaluation of non-Rutherford proton elastic scattering cross section for carbon, *Nucl. Instrum. Methods Phys. Res., Sect. B,* **136-138** (1998) 60-65

18 A.F. Gurbich, Comment on "Carbon analysis using energetic ion beams" [Nucl. Instr. and Meth. B 222 (2004) 538–546], *Nucl. Instrum. Methods Phys. Res., Sect. B,* **229** (2005) 157-158

19 Grime GW, The " Q factor" method: quantitative microPIXE analysis using RBS normalisation, *Nucl. Instrum. Methods Phys. Res., Sect. B,* **109** (1996) 170-174

20 Blaauw M, Campbell JL, Fazinic S, Jaksić M, Orlić I, Van Espen P, The 2000 IAEA intercomparison of PIXE spectrum analysis software, *Nucl. Instrum. Methods Phys. Res., Sect. B,* **189** (2002) 113-122

21 A. Gurbich, C. Jeynes, Evaluation of non-Rutherford proton elastic scattering cross section for magnesium, *Nucl. Instrum. Methods Phys. Res., Sect. B,* **265** (2007) 447-452

22 Pascual-Izarra C, Reis MA, Barradas NP, Simultaneous PIXE and RBS data analysis using Bayesian inference with the DataFurnace code, *Nucl. Instrum. Methods Phys. Res., Sect. B,* **249** (2006) 780-783

23 Jeynes C, Barradas NP, Marriott PK, Boudreault G, Jenkin M, Wendler E, Webb RP, Elemental thin film depth profiles by ion beam analysis using simulated annealing—a new tool, *J. Phys. D: Appl. Phys.* **36** (2003) R97-R126

24 Barradas NP, Arstila K, Battistig G, Bianconi M, Dytlewski N, Jeynes C, Kótai E, Lulli G, Mayer M, Rauhala E, Szilágyi E, Thompson M, Summary of "International Atomic Energy Agency intercomparison of ion beam analysis software". *Nucl. Instrum. Methods Phys. Res., Sect. B,* **266** (2008) 1338-1342

25 Reis MA, Alves LC, Jesus AP, Matrix effects correction for quantitative TTPIXE analysis, *Nucl. Instrum. Methods Phys. Res., Sect. B,* **109/110** (1996) 134-138

26 Maxwell J, Teesdale W, Campbell J, The Guelph PIXE software package II, *Nucl. Instrum. Methods Phys. Res., Sect. B,* **95** (1995) 407-421

27 Barradas NP, Jeynes C, Advanced physics and algorithms in the IBA DataFurnace, *Nucl. Instrum. Methods Phys. Res., Sect. B,* **266** (2008) 1875-1879

28 The SRIM (Stopping and Ranges of Ions in Matter) website, 2008, http://www.srim.org/ [14 June 2008]

29 Ziegler JF, SRIM-2003, *Nucl. Instrum. Methods Phys. Res., Sect. B,* **219** (2004) 1027-1036

30 Ziegler JF, Biersack JP, Ziegler MD, *SRIM - The Stopping and Range of Ions in Matter*, http://www.lulu.com/content/1524197 , 2008

31 The IAEA Nuclear Data Section SigmaCalc website, 2008, http://www-nds.iaea.org/sigmacalc/ [14 June 2008]

32 A. Gurbich, I. Bogdanović-Radović, M. Chiari, C. Jeynes, M. Kokkoris, A.R. Ramos, M. Mayer, E. Rauhala, O. Schwerer, Shi Liqun, I. Vickridge, Status of the problem of nuclear cross section data for IBA, *Nucl. Instrum. Methods Phys. Res., Sect. B,* **266** (2008) 1198-1202

33 Gurbich AF, Evaluation of non-Rutherford proton elastic scattering cross section for oxygen. *Nucl. Instrum. Methods Phys. Res., Sect. B,* **129** (1997) 311-316

34 A. F. Gurbich, Evaluation of non-Rutherford proton elastic scattering cross section for silicon, *Nucl. Instrum. Methods Phys. Res., Sect. B,* **145** (1998) 578-583

35 A. F. Gurbich, N. P. Barradas, C. Jeynes, E. Wendler, Applying elastic backscattering spectrometry when the nuclear excitation function has a fine structure, *Nucl. Instrum. Methods Phys. Res., Sect. B,***190** (2002) 237-240

36 N.P. Barradas, Rutherford backscattering analysis of thin films and superlattices with roughness, *J. Phys. D: Appl. Phys*.,**34** (2001) 2109-2116

37 N. P. Barradas, Fitting of RBS data including roughness: Application to Co/Re multilayers, *Nucl. Instrum. Methods Phys. Res., Sect. B,* **190** (2002) 247-251

38 L. Wielopolski, R.P. Gardner , Prediction of pulse-height spectral distortion caused by peak pile-up effect, *Nucl. Instrum. Methods Phys. Res.*, **133** (1976) 303-309.

39 I.Bogdanović, S.Fazinić, M.Jakšić, T.Tadi, O.Valković, V.Valković, Proton elastic scattering from Fl, Cl, Zn, Se & Br in the energy region 2.5-4.8MeV, *Nucl. Instrum Methods Phys. Res., Sect. B*, **79** (1993) 524-526

40 K.T.Howard, Physical Distribution Trends in Darwin Glass, *Meteoritics and Planetary Science,* **44(2)** (2009) in press

41 S. L. Molodtsov, A. F. Gurbich and C. Jeynes, "Accurate ion beam analysis in the presence of surface roughness", *J. Phys. D: Appl. Phys.,* **41** (2008) 205303 (7pp)